Downloaded from orbit.dtu.dk on: Apr 24, 2024

DTU Library

Delineating papillary dermis around basal cell carcinomas by high and ultrahigh resolution optical coherence tomography - a pilot study

Møller Israelsen, Niels; Mogensen, Mette; Jensen, Mikkel; Haedersdal, Merete; Bang, Ole

Published in:
journal of biophotonics

Link to article, DOI:
10.1002/jbio.202100083

Publication date:
2021

Document Version
Peer reviewed version

Link back to DTU Orbit

Citation (APA):
Møller Israelsen, N., Mogensen, M., Jensen, M., Haedersdal, M., & Bang, O. (2021). Delineating papillary dermis around basal cell carcinomas by high and ultrahigh resolution optical coherence tomography - a pilot study. *journal of biophotonics*, *14*(11), Article e202100083. https://doi.org/10.1002/jbio.202100083

General rights
Copyright and moral rights for the publications made accessible in the public portal are retained by the authors and/or other copyright owners and it is a condition of accessing publications that users recognise and abide by the legal requirements associated with these rights.

- Users may download and print one copy of any publication from the public portal for the purpose of private study or research.
- You may not further distribute the material or use it for any profit-making activity or commercial gain
- You may freely distribute the URL identifying the publication in the public portal

If you believe that this document breaches copyright please contact us providing details, and we will remove access to the work immediately and investigate your claim.

Check for updates

Møller Israelsen Niels (Orcid ID: 0000-0001-9632-7902)

Article type: Original Article

Delineating papillary dermis around basal cell carcinomas by high and ultrahigh resolution optical coherence tomography – a pilot study

Niels Møller Israelsen[1]*, Mette Mogensen[2], Mikkel Jensen[1], Merete Haedersdal[2], Ole Bang[1,3]

*nikr@fotonik.dtu.dk

[1] DTU Fotonik, Department of Photonics Engineering, Technical University of Denmark, Ørsteds Plads, 2800 Kongens Lyngby, Denmark.

[2]Department of Dermatology, Bisbebjerg Hospital, University Hospitals of Copenhagen. Bispebjerg Bakke 23, DK-2400 Copenhagen NV, Denmark

[3]NKT Photonics A/S, Blokken 84, 3460 Birkerød, Denmark.

Abstract

Bedside diagnosis of skin cancer remains a challenging task. The real-time non-invasive technology of optical coherence tomography (OCT) masters a high diagnostic accuracy in basal cell carcinoma (BCC) but a lower specificity in recognizing imitators and other carcinomas. We investigate the delicate signal of papillary dermis using an in-house developed ultrahigh resolution OCT (UHR-OCT) system with shadow compensation and a commercial multi-focus high resolution OCT (HR-OCT) system for clinical BCC imaging. We find that the HR-OCT system struggled to resolve the dark band signal of papillary dermis where the UHR-OCT located this in all cases and detected changes in signal width. UHR-OCT is able to monitor extension and position of papillary dermis suggesting a novel feature for delineating superficial BCCs in pursuit of a fast accurate diagnosis. Comprehensive studies involving more patients are imperative in order to corroborate results.

This article has been accepted for publication and undergone full peer review but has not been through the copyediting, typesetting, pagination and proofreading process which may lead to differences between this version and the Version of Record. Please cite this article as doi: 10.1002/jbio.202100083

This article is protected by copyright. All rights reserved.

Accepted Article

Keywords: Angiography, basal cell carcinoma; BCC; OCT; optical coherence tomography, papillary dermis; ultrahigh resolution; upper dermis.

Abbreviations: BCC, basal cell carcinoma; **DEJ,** dermoepidermal junction; **HR-OCT,** high resolution OCT; **OCT,** optical coherence tomography; **OCTA,** OCT angiography; **RCM,** reflective confocal microscopy; **UHR-OCT,** ultrahigh resolution OCT;

INTRODUCTION

For doctors working with skin cancer, a rapid and accurate diagnosis of a suspicious skin lesion is highly coveted. Portfolios of non-invasive diagnostic scanning devices are available based on either ultrasound, magnetic resonance or light. Such imaging technologies perform swift mapping of tissue, often providing diagnostic information within a few minutes. Keratinocyte carcinomas such as basal cell carcinoma (BCC) are the most frequent type of skin carcinomas in people with light skin types. Non-invasive diagnostics and margin delineation are highly warranted for planning of treatment in these frequently occurring tumours[1].

Optical coherence tomography (OCT) has been known since the beginning of the 90's and traditionally the technology positions itself between reflectance confocal microscopy (RCM) and ultrasound imaging when resolution and penetration depth are used as measures. Typically, near-infrared light is exploited and yields a penetration depth of 1-2 mm and a resolution of 5-10 µm with a single scan probing a skin area of the size of a several square-millimeters. OCT is fast and volume scans can be performed in a few seconds [2]. With commercialization of supercontinuum light sources [3], the depth (axial) resolution of OCT has been pushed towards the single cell level during the last decades introducing *ultrahigh* resolution (UHR), commonly defined as $\delta z < 5\ \mu m$, where δz is the axial resolution. In 2012 the first clinical UHR-OCT studies within dermatology were published, which demonstrated an

Accepted Article

increased diagnostic accuracy as a result of the improved resolution of 3 µm in tissue, both laterally and axially [4–6], the product unfortunately terminated a few years after[7]. Subsequently, a number of applications in the clinic have found use in exploiting UHR-OCT [6,8,9], with the latest commercial UHR-OCT scanner for dermatology, line Field OCT (LC-OCT), Damae, France, promising an impressive isotropic resolution of 1 µm in tissue, thereby resolving single cells [7]. The fine resolution is however achieved on the expense of penetration depth in using a tighter laser beam focus and a center wavelength of ~800 nm whereby only skin depths of 300-400 µm[10] can be reached, also found in case reports[10,11]. Despite that UHR-OCT is now competing with RCM in resolution, delineation of the dermo-epidermal junction (DEJ) is contradictive in LC-OCT images from study to study. A clinical study from 2018 carefully evaluates the DEJ delineation of healthy skin with UHR-OCT suggesting that the papillary dermis, positioned just below the DEJ, appears as a dark band and with this fixes the exact position of the DEJ in UHR-OCT images [12].

In this work we investigate the dark band signal of the papillary dermis in the context of superficially located BCC lesions using an UHR-OCT system mastering a penetration depth of 700 µm, and find the papillary dermis to be a precise depth marker for superficially located BCC and for clear distinction of nodular BCC in expanding into epidermis. We study three BCC lesions and relate the dark band signal of the papillary dermis to the BCC subtype in question. To support our UHR-OCT findings, the same lesions are imaged with a commercial high-resolution (HR) OCT system. In one BCC lesion the OCT angiography functionality is demonstrated to enhance the diagnostic power, which has been demonstrated in a number of clinical studies [13–16].

MATERIALS AND METHODS

In this pilot study two OCT systems were applied. One UHR-OCT system constructed in-house with an axial/lateral resolution of 2µm/6µm (in tissue). The second system is a

Accepted Article

commercial multi-focus HR OCT system, VivoSight, from Michelson Diagnostics, producing an axial/lateral resolution of 5µm/7.5µm (in tissue). Both systems were interfaced with handheld probes illuminating with 5 mW average power of light with center wavelength of about ~1300 nm. The axial alignment was done with a commercial hollow alignment spacer matching the skin-area and patient for the HR-OCT system, while the UHR-OCT interfaced the patient with a window covered with certified palm oil. In operation, the HR-OCT system scanned an area of 6 mm x 6 mm where the UHR-OCT system covered a skin area of 3 mm x 3 mm.

In creating the UHR-OCT images, dispersion compensation and shadow compensation (DC) were carried out [12,17]. The DC was only of the mono-depth kind, as all-depth DC was found redundant due to the low dispersion in human tissue in the 1300 nm wavelength regime [18]. All morphology cross-section images presented are averages of five single B-scans. From the same dataset, OCT angiography (OCTA) images were generated. Speckle based OCTA [19] was applied and evaluated over five consecutive B-scans. OCTA images were constructed as follows. First a Gaussian spatial filter was deployed to single B-scan images, speckle variance was calculated, smoothing of the speckle variance image was performed with a Wiener filter and finally a lower thresholding of the OCTA signal was introduced. The OCTA signal was overlaid on the structural signal thereby forming the composite images that are from now on referred to as OCTA images. For the HR-OCT system, the 'Dynamic OCT' feature was applied to give similar OCTA images.

The study consecutively included patients from the skin cancer clinic at Dept. of Dermatology, Bispebjerg Hospital, Copenhagen on October 7th, 2019. Six patients, age 73-85 years, with BCC lesions confirmed by histopathology were OCT scanned prior to Mohs surgery or radiation therapy. Adjacent healthy skin was also included in the scans. This case series is part of a larger study approved by the local Ethics committee (Journal no. H-19036900). Written and oral informed consent were obtained before enrolment in study

Accepted Article

conducted in accordance with the Declaration of Helsinki.

In diagnosing and subtyping BCCs, imitators and other keratinocyte carcinomas, many parameters have been reported in OCT literature. More systematically, two diagnostic algorithms have been defined for recognizing and distinguishing BCCs [20,21]. In the following, we apply terms utilized in these algorithms to describe our observations: BCC islands in the skin appear as dark grey oval structures, with the characteristic hyper-reflective halo. A dark to black signal layer surrounding BCC islands are known in the literature as *clefting*, a phenomenon where the tumor cell aggregation retracts and detaches from the interfacing healthy cells giving space to peritumoral mucin building, forming a cleft-like rim embracing the tumor [22]. Both preceding RCM and OCT studies show that clefting is seen as a dark peritumoural ribbon/margin/band [22,23].

RESULTS AND DISCUSSION

Due to challenges with either interfacing or alignment of the UHR-OCT probe, only OCT images from three of the six patients scanned presented a proper scan encompassing the BCC regions.

Heathy skin

To visualize the dark band signal (DB) of papillary dermis as a reference to our BCC observations presented and discussed subsequently in the manuscript, we present an example on healthy skin. The example is given in **Figure 1(a)** and **(b)**. In HR- OCT and UHR-OCT B-scans both the epidermis and dermis signals are recognized commonly known for their respective weaker and stronger signals. The relative difference is known from the fact that reticular dermis holds closely packed collagen fibers and comprise various adnexal structures and blood vessels that are manifested as highly scattering objects. The epidermis signal is primarily provided by intra- and intercellular interfaces. What is apparent in the UHR-OCT image, and just noticeable in the HR-OCT image, is also an even darker signal band (the DB)

Accepted Article

Accepted Article

situated in between the traditional epidermis and dermis signals. This DB signal is emphasized in the zoom-ins in **Figure 1(c)** and **(d)** of the boxed regions in Figure 1(a) and (b). This DB has the undulated finger-like feature reaching into the epidermis (as highlighted in Figure 1(d) in magenta). In the structural appearance and knowing the micro-anatomy of the papillary dermis, we suggest that the DB is that of the upper (papillary) dermis naturally on top of the lower (reticular) dermis. The latter is comprised of densely packed collagen fibers and thus presents a hyperreflective layer. Apart from the earlier study by the authors [12], the DB is also well documented in the literature with other types of UHR-OCT systems [20], however in these studies it is just acknowledged and termed ”The sub-basal membrane area”. In the UHR-OCT zoom-in in Figure 1(d), the papillary dermis is highlighted in magenta by a narrow contrast thresholding matching that of the DB. Here the geometrical structure of the papillary dermis is evident with finger-like protrusions towards epidermis while appearing relatively flat towards the reticular dermis. From the zoom-in of the HR-OCT B-scan (Figure 1(c)), the DB can be noticed but the contrast in the transition going from epidermis to dermis is not as pronounced and not surprisingly do not resolve the DB as well either.

An example of the OCTA function of UHR-OCT in healthy skin is given in Figure 1(e) and (f), in-plane and in cross-sectional view of the skin, respectively. With this, larger uniform blood vessel are easily visualized, especially in the *en face* volume segmentations [13].

Basal cell carcinomas

OCT images from a superficially loctaed BCC example are presented in **Figure 2** with the BCC lesion is vaguely seen as a nuance in the surface projection (Figure 2(a)) but uncovered by the C-scan in depth (Figure 2(b)). The BCC cell-cluster appears as a multiple thickening of epidermis taking a similar signal strength to that of epidermis. As a result, the BCC is observed as a ’dark island’ or ’nest’ at the depth level of the reticular dermis in the surrounding healthy tissue, as seen from B-scans of Figure 2(c-d). Noticeable, and boxed (solid lining) in

Figure 2(b-e), is the DB signal of the papillary dermis in both the healthy and the diseased part. In the UHR-OCT images the multifold thickening of the DB signal-width of the tumor island is evident where in the HR-OCT image this transition is less pronounced and primarily seen as a contrast improvement of the DB. The cleft of the tumor is both observed *en face* and cross-sectional in the UHR-OCT images in Figure 2(b-d). The transition from a healthy epidermis to that merged with the BCC is however only seen in the cross-sectional images. The BCC tumor depth were found to a level of ~500 µm.

A nodular BCC is visualized in **Figure 3**. Tumor aggregations are smaller and more scattered and again seen as dark islands, however appearing as dark oval structures (ovoids), with characteristic hyperreflective top entrance signal, seen in both UHR-OCT and HR-OCT images in Figure3(c-f). Tumor necrosis is also observed by both OCT systems as even darker islands within the BCC but containing hyper-reflective flickers representing tumor debris (marked 'N' in Figure 3(c), (d) and (f)).

The third BCC example, also a nodular BCC, is given in **Figure 4**. This BCC resembles that displayed in Figure 3 as dark islands appear below the DEJ possessing the hyper-reflective entrance signal as depicted in Figure 3 (c-e). However, in Figure 4 the upper boundary of the BCCs are found remote from the DEJ (more than 100 µm in depth) and BCCs exhibit the largest dimension in the lateral plane. Due to the potential deep location, it is also easily confused with blood vessels and adnexal structures giving a similar dark signal. For this BCC, the DB signal of the papillary dermis is apparent in the UHR-OCT images and barely visible in the HR-OCT images (Figure 4(c-e)). In the HR-OCT image, one BCC is in vicinity of the DEJ where the DB signal is absent indicating a more deep-seated lesion.

The link between the BCC of Figure 4 and the basal cell layer is displayed by a custom cross-sectional cut, marked in **Figure 5(a)** by a dotted line and presented in **Figure 5(c)**. Here the dark island in depth is recognized with the characteristic hyperreflective entrance signal (dashed boxed). For the specific cross-sectional segment, the connection between the

Accepted Article

suspected BCC and a hair follicle is marked (circled).

In Figure 5(a), the structural UHR-OCT *en face* image presented in Figure 4(b), is overlaid with the speckle based OCTA signal. In the image, we observe blood vessels inside the BCC lesion, so called arborizing vessels [6]. The HR-OCT OCTA image of **Figure 5(b)** shows similar pronounced irregular tree-like branching patterns of blood-vessels in the same area; patterns which have been shown as BCC indicators [13,14]. In Figure 3-5 the vertical tumor depths were found to extend to the range 600-700 µm from the skin surface.

Discussion

Basal cell carcinomas (BCC) come in various subtypes, the superficial and nodular being the most common – the morphea-like the most difficult to treat. However up to 25% of BCC lesions are mixed types [24] and in this study we focus on the overall BCC architecture. The BCCs presented here have distinctive appearances. In the image evaluation, the dark band (DB) signal of the papillary dermis has been a subject of measure. In the presented material this signal was effortlessly delineated in the healthy skin UHR-OCT images where only a fraction of the HR-OCT images revealed the presence of the DB signal and thus the papillary dermis, in line with the preceding study [12]. Based on this performance, evaluation of the papillary dermis signal was conducted for three BCCs with focus on the UHR-OCT image material.

In Fig.2 the DB appeared intact. When evaluating Figure 3 and Figure 4, nodular BCCs were, not surprisingly, found underneath the DEJ, seen in the appearance beneath the DB signal of papillary dermis in the UHR-OCT images. The DB was absent for most cases in the HR-OCT images. The dark islands of the BCCs commonly held a hyper-reflective entrance signal and no significant distortion of the DEJ was seen. As BCCs originate from keratinocytes of the basal cell layer, the BCCs found remote to DEJ must stem from adnexal structures retracting the DEJ well into the depth of the dermis. This is also to be expected from

Accepted Article

the BCCs found in the UHR-OCT images of Fig 4. The connection between the BCC and an adnexal structure penetrating into dermis was delineated in a skewed cross-sectional B-scan segment presented in Fig 5(c): the BCC merging with a hair follicle about 300 µm below the skin surface.

Increased interest in OCT angiography (OCTA), also termed 'dynamic OCT', has emerged in clinical dermatology [14]. In OCTA density and morphology of vascular patterns show promising results for increasing accuracy in non-melanoma skin cancer diagnosis [13–16]. The OCTA functionality of blood flow visualization was added to the structural image of Figure 4 and presented in Figure 5 for which well-demarquated blood-vessels were found in the location of the BCCs having a characteristic irregular propagation pattern of arborizing blood vessels. Comparing to the *en face* OCTA view of the HR-OCT in image Figure 5(b), similar blood vessel behavior was seen.

Only recently, the papillary dermis was clearly delineated in OCT images, which is only possible in ultrahigh resolution images [12]. Several UHR-OCT studies demonstrate even better resolution (although poorer penetration depth) [7,25,26,10,27]. However, the majority suggest that DEJ is positioned at the interface to the high reflective layer of reticular dermis; dismissing the single images of dark skin where the basal cell layer is unmistakable due to the high concentration of melanin [26]. The understanding of the DEJ position at the interface of the highly reflective reticular dermis coincides with the general understanding of the community up until now [20,28–33,33,34]. The study here represents the first OCT study where the DB signal of the papillary dermis is utilized in the context of recognizing BCC tumour depth. With the three examples we find that the DB signal enables us to precisely relate the position of a BCC to the DEJ where prior studies have used the entrance to reticular dermis as a guide for locating the DEJ. Additionally UHR-OCT documents in Figure 3 a thinned unbroken papillary dermis; an observation mostly undetected by HR-OCT, however recognized in LC-OCT images of [35], albeit uncommented. Based on these observations the DB signal of

Accepted Article

papillary dermis might serve as an attributing aid for efficiently sub-typing and delineating skin cancers in particular superficially located BCC. Both in manual image inspection but also in automated skin layer delineation with UHR-OCT [36].

Limitations: We only included few BCC lesions in the analysis and for this reason did not differentiate BCC subtypes by quantitative localization of the dermo-epidermal junction in and outside the BCC islands. We found that the UHR-OCT system handheld probe is difficult to position without any guiding aid causing erroneous scans outside the skin lesion area (~50%) and we thus propose to include a guiding camera in the UHR-OCT probe in the subsequent main study.

CONCLUSION

This preliminary clinical study on BCC lesions based on UHR-OCT imaging with shadow compensation present three BCC examples evaluated and compared with cross-sectional scans of a commercial HR-OCT system with an axial resolution more than twice as large of that of the UHR-OCT system. The UHR-OCT system was found to be superior in detecting the DB signal of the papillary dermis in all examples. The HR-OCT system was found to be significantly less sensitive in detecting the DB signal which appeared less clear-cut and changes of this with depth was also difficult to identify. Furthermore, OCTA signals were demonstrated for one BCC lesion and similitude was found for the vascular behavior between the OCTA signals of UHR-OCT and HR-OCT systems.

In OCT images the DB signal of the papillary dermis can serve as an indicator of BCC depth in superficially located BCC lesions and potentially improve treatment planning of BCCs in the future. Since most BCC lesions are thin, our findings are clinically relevant. Importantly, the presence of a normal DEJ junction does not rule out the presence of a deep-seated and potentially aggressive BCC. Hence neither UHR-OCT nor LC-OCT can stand alone in OCT diagnosis and treatment planning of

Accepted Article

BCC lesions[37].

ACKNOWLEDGEMENTS:

We acknowledge support from Innovation Fund Denmark under the project J. No. 4107-00011A (ShapeOCT), Vissing Foundation, Denmark and the Research Foundation of Bispebjerg and Frederiksberg Hospital financing part of Mette Mogensen´s salary.

DATA AVAILABILITY STATEMENT

The data that support the findings of this study are available from the corresponding author upon reasonable request.

CONFLICT OF INTEREST

The authors declare no financial or commercial conflict of interest.

REFERENCES:

(1) Peris, K.; Fargnoli, M. C.; Garbe, C.; Kaufmann, R.; Bastholt, L.; Seguin, N. B.; Bataille, V.; Marmol, V. del; Dummer, R.; Harwood, C. A.; Hauschild, A.; Höller, C.; Haedersdal, M.; Malvehy, J.; Middleton, M. R.; Morton, C. A.; Nagore, E.; Stratigos, A. J.; Szeimies, R.-M.; Tagliaferri, L.; Trakatelli, M.; Zalaudek, I.; Eggermont, A.; Grob, J. J. Diagnosis and Treatment of Basal Cell Carcinoma: European Consensus–Based Interdisciplinary Guidelines. *European Journal of Cancer* **2019**, *118*, 10–34. https://doi.org/10.1016/j.ejca.2019.06.003.

(2) Leitgeb, R. A. En Face Optical Coherence Tomography: A Technology Review [Invited]. *Biomed. Opt. Express* **2019**, *10* (5), 2177. https://doi.org/10.1364/BOE.10.002177.

(3) Petersen, C. R.; Møller, U.; Kubat, I.; Zhou, B.; Dupont, S.; Ramsay, J.; Benson, T.; Sujecki, S.; Abdel-Moneim, N.; Tang, Z.; Furniss, D.; Seddon, A.; Bang, O. Mid-

Accepted Article

Infrared Supercontinuum Covering the 1.4–13.3 Mm Molecular Fingerprint Region Using Ultra-High NA Chalcogenide Step-Index Fibre. *Nature Photon* **2014**, *8* (11), 830–834. https://doi.org/10.1038/nphoton.2014.213.

(4) Blatter, C.; Weingast, J.; Alex, A.; Grajciar, B.; Wieser, W.; Drexler, W.; Huber, R.; Leitgeb, R. A. In Situ Structural and Microangiographic Assessment of Human Skin Lesions with High-Speed OCT. *Biomed. Opt. Express, BOE* **2012**, *3* (10), 2636–2646. https://doi.org/10.1364/BOE.3.002636.

(5) Lee, K.-S.; Zhao, H.; Ibrahim, S. F.; Meemon, N.; Khoudeir, L.; Rolland, J. P. Three-Dimensional Imaging of Normal Skin and Nonmelanoma Skin Cancer with Cellular Resolution Using Gabor Domain Optical Coherence Microscopy. *JBO* **2012**, *17* (12), 126006. https://doi.org/10.1117/1.JBO.17.12.126006.

(6) Ruffano, L. F. di; Dinnes, J.; Deeks, J. J.; Chuchu, N.; Bayliss, S. E.; Davenport, C.; Takwoingi, Y.; Godfrey, K.; O'Sullivan, C.; Matin, R. N.; Tehrani, H.; Williams, H. C.; Group, C. S. C. D. T. A. Optical Coherence Tomography for Diagnosing Skin Cancer in Adults. *Cochrane Database of Systematic Reviews* **2018**, No. 12. https://doi.org/10.1002/14651858.CD013189.

(7) Dubois, A.; Levecq, O.; Azimani, H.; Siret, D.; Barut, A.; Suppa, M.; del Marmol, V.; Malvehy, J.; Cinotti, E.; Rubegni, P.; Perrot, J.-L. Line-Field Confocal Optical Coherence Tomography for High-Resolution Noninvasive Imaging of Skin Tumors. *J. Biomed. Opt.* **2018**, *23* (10), 1. https://doi.org/10.1117/1.JBO.23.10.106007.

(8) Mogensen, M.; Bojesen, S.; Israelsen, N. M.; Maria, M.; Jensen, M.; Podoleanu, A.; Bang, O.; Haedersdal, M. Two Optical Coherence Tomography Systems Detect Topical Gold Nanoshells in Hair Follicles, Sweat Ducts and Measure Epidermis. *Journal of Biophotonics* **2018**, *11* (9), e201700348. https://doi.org/10.1002/jbio.201700348.

(9) Rajabi-Estarabadi, A.; Bittar, J. M.; Zheng, C.; Nascimento, V.; Camacho, I.; Feun, L. G.; Nasiriavanaki, M.; Kunz, M.; Nouri, K. Optical Coherence Tomography Imaging of Melanoma Skin Cancer. *Lasers Med Sci* **2019**, *34* (2), 411–420. https://doi.org/10.1007/s10103-018-2696-1.

(10) Tognetti, L.; Cinotti, E.; Suppa, M.; Guazzo, R.; Habougit, C.; Santi, F.; Diet, G.; Fontaine, M.; Berot, V.; Monnier, J.; Pianigiani, E.; Marmol, V. del; Malvehy, J.; Perrot, J.-L.; Rubegni, P. Line Field Confocal Optical Coherence Tomography: An Adjunctive Tool in the Diagnosis of Autoimmune Bullous Diseases. *Journal of Biophotonics n/a* (n/a), e202000449. https://doi.org/10.1002/jbio.202000449.

Accepted Article

Accepted Article

(11) Lacarrubba, F.; Verzì, A. E.; Puglisi, D. F.; Micali, G. Line-Field Confocal Optical Coherence Tomography: A Novel, Non-Invasive Imaging Technique for a Rapid, in-Vivo Diagnosis of Herpes Infection of the Skin. *Journal of the European Academy of Dermatology and Venereology n/a* (n/a). https://doi.org/10.1111/jdv.17182.

(12) Israelsen, N. M.; Maria, M.; Mogensen, M.; Bojesen, S.; Jensen, M.; Haedersdal, M.; Podoleanu, A.; Bang, O. The Value of Ultrahigh Resolution OCT in Dermatology - Delineating the Dermo-Epidermal Junction, Capillaries in the Dermal Papillae and Vellus Hairs. *Biomed. Opt. Express, BOE* **2018**, *9* (5), 2240–2265. https://doi.org/10.1364/BOE.9.002240.

(13) Olsen, J.; Holmes, J.; Jemec, G. B. E. Advances in Optical Coherence Tomography in Dermatology—a Review. *JBO* **2018**, *23* (4), 040901. https://doi.org/10.1117/1.JBO.23.4.040901.

(14) Sigsgaard, V.; Themstrup, L.; Riis, P. T.; Olsen, J.; Jemec, G. B. In Vivo Measurements of Blood Vessels' Distribution in Non-Melanoma Skin Cancer by Dynamic Optical Coherence Tomography — a New Quantitative Measure? *Skin Research and Technology* **2018**, *24* (1), 123–128. https://doi.org/10.1111/srt.12399.

(15) Levine, A.; Wang, K.; Markowitz, O. Optical Coherence Tomography in the Diagnosis of Skin Cancer. *Dermatol Clin* **2017**, *35* (4), 465–488. https://doi.org/10.1016/j.det.2017.06.008.

(16) Themstrup, L.; Carvalho, N. D.; Nielsen, S. M.; Olsen, J.; Ciardo, S.; Schuh, S.; Nørnberg, B. M.-H.; Welzel, J.; Ulrich, M.; Pellacani, G.; Jemec, G. B. E. In Vivo Differentiation of Common Basal Cell Carcinoma Subtypes by Microvascular and Structural Imaging Using Dynamic Optical Coherence Tomography. *Experimental Dermatology* **2018**, *27* (2), 156–165. https://doi.org/10.1111/exd.13479.

(17) Bradu, A.; Israelsen, N. M.; Maria, M.; Marques, M. J.; Rivet, S.; Feuchter, T.; Bang, O.; Podoleanu, A. Recovering Distance Information in Spectral Domain Interferometry. *Scientific Reports* **2018**, *8* (1), 1–16. https://doi.org/10.1038/s41598-018-33821-0.

(18) Jensen, M.; Israelsen, N. M.; Maria, M.; Feuchter, T.; Podoleanu, A.; Bang, O. All-Depth Dispersion Cancellation in Spectral Domain Optical Coherence Tomography Using Numerical Intensity Correlations. *Scientific Reports* **2018**, *8* (1), 1–10. https://doi.org/10.1038/s41598-018-27388-z.

(19) Chen, C.-L.; Wang, R. K. Optical Coherence Tomography Based Angiography [Invited]. *Biomed. Opt. Express, BOE* **2017**, *8* (2), 1056–1082. https://doi.org/10.1364/BOE.8.001056.

Accepted Article

(20) Boone, M. a. L. M.; Suppa, M.; Pellacani, G.; Marneffe, A.; Miyamoto, M.; Alarcon, I.; Ruini, C.; Hofmann-Wellenhof, R.; Malvehy, J.; Jemec, G. B. E.; Marmol, V. D. High-Definition Optical Coherence Tomography Algorithm for Discrimination of Basal Cell Carcinoma from Clinical BCC Imitators and Differentiation between Common Subtypes. *Journal of the European Academy of Dermatology and Venereology* **2015**, *29* (9), 1771–1780. https://doi.org/10.1111/jdv.13003.

(21) Wahrlich, C.; Alawi, S. A.; Batz, S.; Fluhr, J. W.; Lademann, J.; Ulrich, M. Assessment of a Scoring System for Basal Cell Carcinoma with Multi-Beam Optical Coherence Tomography. *Journal of the European Academy of Dermatology and Venereology* **2015**, *29* (8), 1562–1569. https://doi.org/10.1111/jdv.12935.

(22) Ulrich, M.; Roewert-Huber, J.; González, S.; Rius- Diaz, F.; Stockfleth, E.; Kanitakis, J. Peritumoral Clefting in Basal Cell Carcinoma: Correlation of in Vivo Reflectance Confocal Microscopy and Routine Histology. *Journal of Cutaneous Pathology* **2011**, *38* (2), 190–195. https://doi.org/10.1111/j.1600-0560.2010.01632.x.

(23) Yücel, D.; Themstrup, L.; Manfredi, M.; Jemec, G. B. E. Optical Coherence Tomography of Basal Cell Carcinoma: Density and Signal Attenuation. *Skin Res Technol* **2016**, *22* (4), 497–504. https://doi.org/10.1111/srt.12291.

(24) Wu, A.; Sun, M. T.; Huilgol, S. C.; Madge, S.; Selva, D. Histological Subtypes of Periocular Basal Cell Carcinoma. *Clinical & Experimental Ophthalmology* **2014**, *42* (7), 603–607. https://doi.org/10.1111/ceo.12298.

(25) Dubois, A.; Levecq, O.; Azimani, H.; Davis, A.; Ogien, J.; Siret, D.; Barut, A. Line-Field Confocal Time-Domain Optical Coherence Tomography with Dynamic Focusing. *Opt. Express, OE* **2018**, *26* (26), 33534–33542. https://doi.org/10.1364/OE.26.033534.

(26) Davis, A.; Levecq, O.; Azimani, H.; Siret, D.; Dubois, A. Simultaneous Dual-Band Line-Field Confocal Optical Coherence Tomography: Application to Skin Imaging. *Biomed. Opt. Express, BOE* **2019**, *10* (2), 694–706. https://doi.org/10.1364/BOE.10.000694.

(27) Ogien, J.; Levecq, O.; Cazalas, M.; Suppa, M.; Marmol, V. del; Malvehy, J.; Cinotti, E.; Rubegni, P.; Perrot, J.-L.; Dubois, A. Handheld Line-Field Confocal Optical Coherence Tomography for Dermatology. In *Photonics in Dermatology and Plastic Surgery 2020*; International Society for Optics and Photonics, 2020; Vol. 11211, p 112110S. https://doi.org/10.1117/12.2545546.

(28) Welzel, J.; Lankenau, E.; Birngruber, R.; Engelhardt, R. Optical Coherence Tomography of the Human Skin. *Journal of the American Academy of Dermatology*

1997, *37* (6), 958–963. https://doi.org/10.1016/S0190-9622(97)70072-0.

(29) Boone, M. A. L. M.; Norrenberg, S.; Jemec, G. B. E.; Marmol, V. D. Imaging Actinic Keratosis by High-Definition Optical Coherence Tomography. Histomorphologic Correlation: A Pilot Study. *Experimental Dermatology* **2013**, *22* (2), 93–97. https://doi.org/10.1111/exd.12074.

(30) Boone, M.; Norrenberg, S.; Jemec, G.; Del Marmol, V. High-Definition Optical Coherence Tomography: Adapted Algorithmic Method for Pattern Analysis of Inflammatory Skin Diseases: A Pilot Study. *Arch Dermatol Res* **2013**, *305* (4), 283–297. https://doi.org/10.1007/s00403-012-1311-8.

(31) Boone, M. A. L. M.; Norrenberg, S.; Jemec, G. B. E.; Marmol, V. D. High-Definition Optical Coherence Tomography Imaging of Melanocytic Lesions: A Pilot Study. *Arch Dermatol Res* **2014**, *306* (1), 11–26. https://doi.org/10.1007/s00403-013-1387-9.

(32) Boone, M. a. L. M.; Marneffe, A.; Suppa, M.; Miyamoto, M.; Alarcon, I.; Hofmann-Wellenhof, R.; Malvehy, J.; Pellacani, G.; Marmol, V. D. High-Definition Optical Coherence Tomography Algorithm for the Discrimination of Actinic Keratosis from Normal Skin and from Squamous Cell Carcinoma. *Journal of the European Academy of Dermatology and Venereology* **2015**, *29* (8), 1606–1615. https://doi.org/10.1111/jdv.12954.

(33) Boone, M. A. L. M.; Suppa, M.; Dhaenens, F.; Miyamoto, M.; Marneffe, A.; Jemec, G. B. E.; Del Marmol, V.; Nebosis, R. In Vivo Assessment of Optical Properties of Melanocytic Skin Lesions and Differentiation of Melanoma from Non-Malignant Lesions by High-Definition Optical Coherence Tomography. *Arch Dermatol Res* **2016**, *308* (1), 7–20. https://doi.org/10.1007/s00403-015-1608-5.

(34) Boone, M. A. L. M.; Suppa, M.; Marneffe, A.; Miyamoto, M.; Jemec, G. B. E.; Del Marmol, V. High-Definition Optical Coherence Tomography Intrinsic Skin Ageing Assessment in Women: A Pilot Study. *Arch Dermatol Res* **2015**, *307* (8), 705–720. https://doi.org/10.1007/s00403-015-1575-x.

(35) Suppa, M.; Fontaine, M.; Dejonckheere, G.; Cinotti, E.; Yélamos, O.; Diet, G.; Tognetti, L.; Miyamoto, M.; Cano, C. O.; Perez-Anker, J.; Panagiotou, V.; Trepant, A. L.; Monnier, J.; Berot, V.; Puig, S.; Rubegni, P.; Malvehy, J.; Perrot, J. L.; Marmol, V. del. Line-Field Confocal Optical Coherence Tomography of Basal Cell Carcinoma: A Descriptive Study. *Journal of the European Academy of Dermatology and Venereology* **2021**, *35* (5), 1099–1110. https://doi.org/10.1111/jdv.17078.

(36) del Amor, R.; Morales, S.; Colomer, A.; Mogensen, M.; Jensen, M.; Israelsen, N. M.;

Accepted Article

Bang, O.; Naranjo, V. Automatic Segmentation of Epidermis and Hair Follicles in Optical Coherence Tomography Images of Normal Skin by Convolutional Neural Networks. *Front. Med.* **2020**, *7*. https://doi.org/10.3389/fmed.2020.00220.

(37) Walling, H. W.; Fosko, S. W.; Geraminejad, P. A.; Whitaker, D. C.; Arpey, C. J. Aggressive Basal Cell Carcinoma: Presentation, Pathogenesis, and Management. *Cancer Metastasis Rev* **2004**, *23* (3), 389–402. https://doi.org/10.1023/B:CANC.0000031775.04618.30.

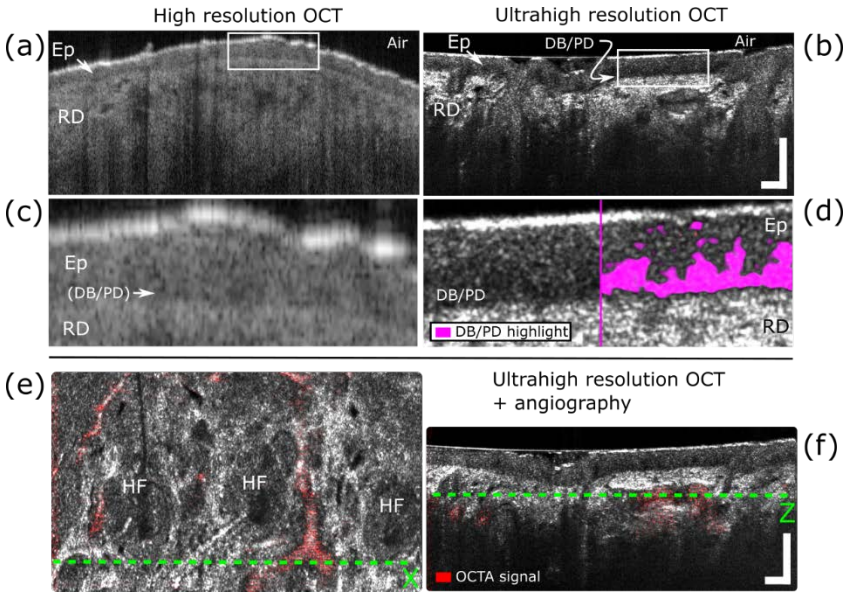

FIGURE 1. OCT images of healthy skin (behind ear), which is defined by two layers: epidermis and dermis separated by the dermo-epidermal junction (DEJ). Our focus is the dark band (DB) signal of upper (papillary) dermis. TOP: Skin layers delineation in (a) HR-OCT and (b) UHR-OCT images (Ep = epidermis, DB= dark band signal, RD = reticular lower dermis). Boxed regions are highlighted in (c-d) zoom-ins below. CENTER (c) HR-OCT and (d) UHR-OCT zoom-ins where DB for the latter is highlighted with magenta using simple contrast thresholding after a bandpass filter for diminishing speckle patterns. BOTTOM: (e) en face and (f) cross-sectional UHR-OCT angiography. Mutual segmentations are marked with dashed lines and hair follicles are indicated (HF). Patient data: 73 y. male. Scale bars represent 200 µm.

Accepted Article

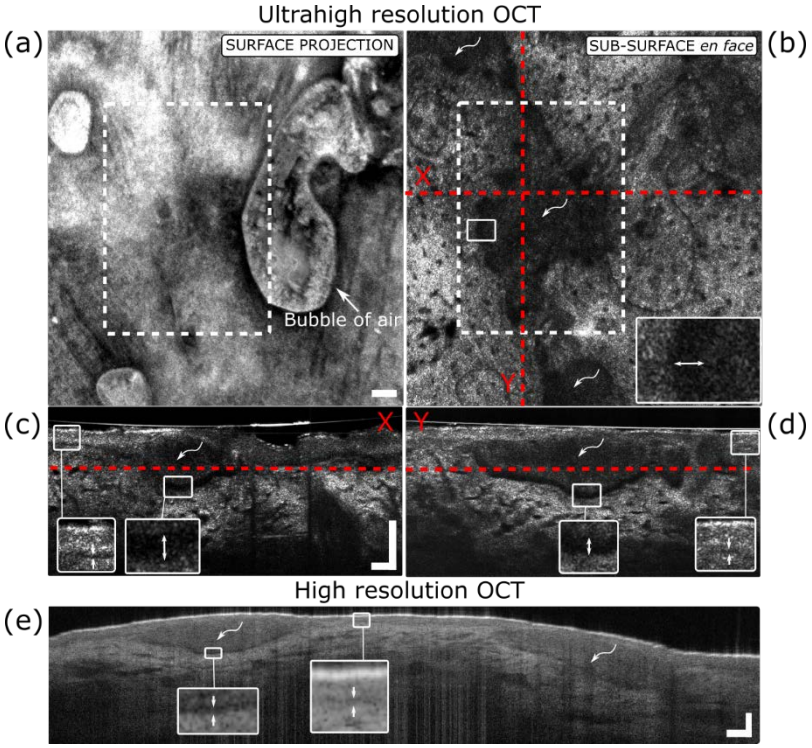

FIGURE 2. OCT images of a superficial BCC on the shoulder. TOP: (a) Surface projection, (b) en face view, (c-d) cross-sectional views of UHR-OCT scan. Square dashed box is a guide to the eye. Mutual segmentations are marked with dashed lines. BOTTOM: (e) HR-OCT cross-section for comparison. Hard boxed regions are highlighted to mark papillary dermis/dark band signal (double arrows). Wriggly arrows pinpoint dark BCC cell islands. Patient data: 76 y. male. Scale bars represent 200 µm.

Accepted Article

Accepted Article

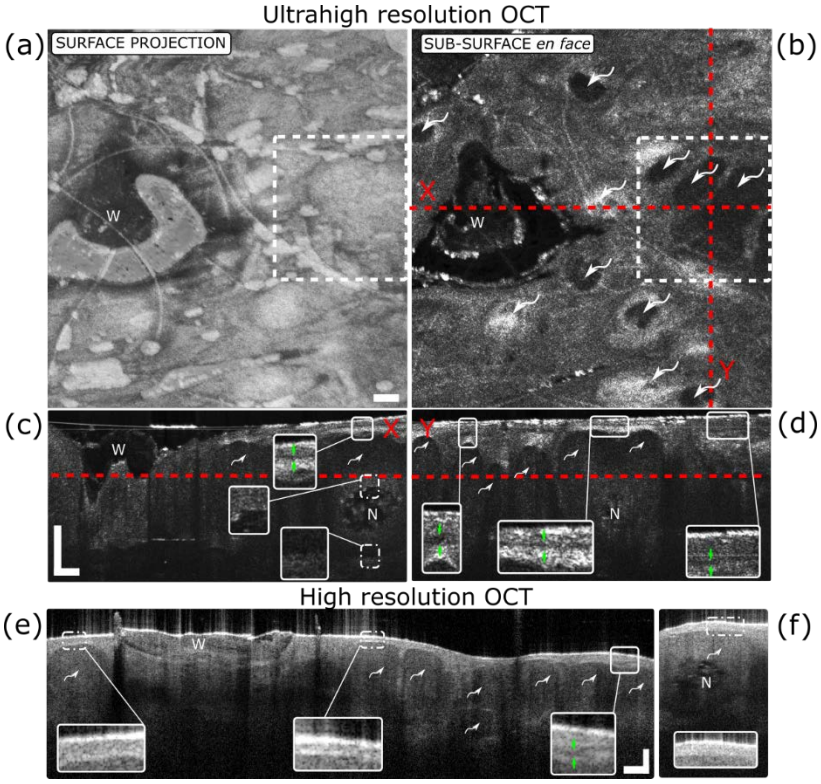

FIGURE 3. OCT images of a facial nodular BCC. TOP: (a) Surface projection, (b) en face view, (c-d) cross-sectional views of UHR-OCT scan. Square dashed box is a guide to the eye. Mutual segmentations are marked with dashed lines. BOTTOM: (e-f) two different HR-OCT cross-section of the same volume scan for comparison. Hard boxed regions are highlighted to mark papillary dermis/dark band signal (double arrows) while dashed/dotted boxes highlight boundary and intra-tumor signal transitions. Wriggly arrows pinpoint dark ovoid BCC cell islands, 'W' marks wound crust and 'N' marks tumor necrosis. Patient data: 65 y. female. . Scale bars represent 200 µm.

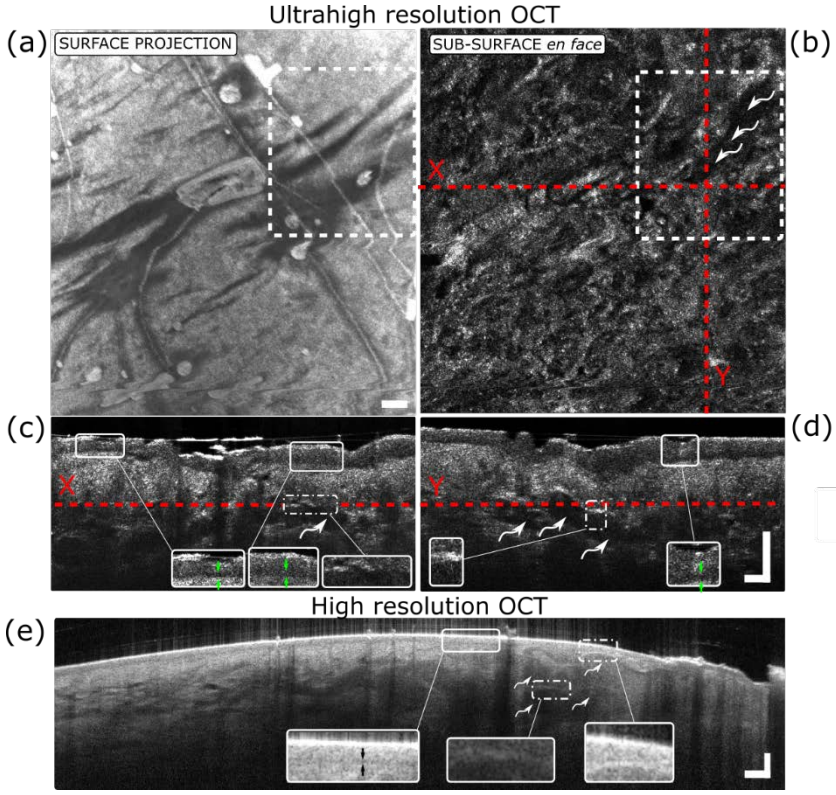

FIGURE 4. OCT images of a facial nodular BCC. TOP: (a) Surface projection, (b) en face view, (c-d) cross-sectional views of UHR-OCT scan. Square dashed box is a guide to the eye. Mutual segmentations are marked with dashed lines. BOTTOM: (e) HR-OCT cross-section for comparison. Hard boxed regions are highlighted to mark papillary dermis/dark band signal (double arrows) while dashed/dotted boxes highlight boundary and intra-tumor signal transitions. Wriggly arrows pinpoint dark ovoid BCC aggregations. Patient data: 85 y. female. Scale bars represent 200 µm.

Accepted Article

Accepted Article

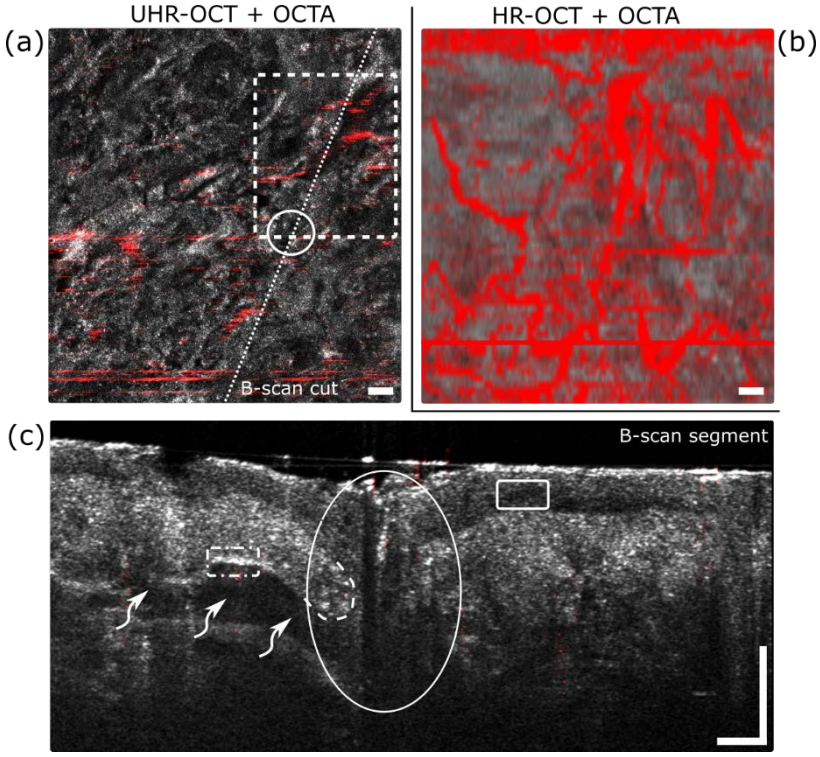

FIGURE 5. OCTA image of BCC temple region. TOP: (a) UHR-OCT and (b) HR-OCT OCTA en faces images. Dashed box markes region of interest seen in Figure 4. BOTTOM: (c) Cross-sectional cut marked in en face image as dotted line. Circles embrace hair follicle of interest for which suspected BCC emanate. Wriggly arrows point out dark BCC aggregations. Red color show OCTA signals. Hard boxed regions are highlighted to mark papillary dermis/dark band signal. Patient data: same as Fig.4. Scale bars represent 200 µm. Horizontal red lines in (a) and (b) are image artifacts.